

Further results on the development of a novel VTOL aircraft, the Anuloid. Part II: Flight mechanics

Marco Petrolo^{*1}, Erasmo Carrera^{1a}, Coen de Visser^{2b}, Michele D'Ottavio^{3c}
and Olivier Polit^{3d}

¹MUL2 Group, Department of Mechanical and Aerospace Engineering, Politecnico di Torino,
Corso Duca degli Abruzzi 24, Torino, Italy

²Control and Simulation Division, Faculty of Aerospace Engineering, Delft University of Technology,
Delft 2600GB, The Netherlands

³Laboratoire Energétique, Mécanique et Electromagnétisme (LEME), Université Paris Ouest,
50 rue de Sèvres, 92410 Ville d'Avray, France

(Received June 27, 2016, Revised June 30, 2016, Accepted July 8, 2016)

Abstract. This paper presents the main outcomes of the preliminary development of the Anuloid, an innovative disk-shaped VTOL aircraft. The Anuloid has three main features: lift is provided by a ducted fan powered by a turboshaft; control capabilities and anti-torque are due to a system of fixed and movable surfaces that are placed in the circular internal duct and the bottom portion of the aircraft; the Coanda effect is exploited to enable the control capabilities of such surfaces. In this paper, results from flight mechanics are presented. The vertical flight dynamics were found to be desirable. In contrast, the horizontal flight dynamics of the aircraft shows both dynamic instability, and more importantly, insufficient pitch and roll control authority. Some recommendations and guidelines are then given aimed at the alleviation of such problems.

Keywords: VTOL; Coanda effect; flyability

1. Introduction to VTOL aircraft

Vertical Take-Off and Landing (VTOL) airplanes are particularly interesting since they can take-off and land in limited spaces, do not need classical airport installations and dedicated runways, and have enhanced versatility. On the other hand, the development of a VTOL leads to some critical issues. Such as the vertical and horizontal flight efficiency, transition phases, the flight control authority, and noise (Lindenbaum 1986).

Helicopters are the most common and successful type of VTOL. They are used for civil and military applications, and, in particular, for emergency operations in urban areas, offshore

*Corresponding author, Assistant Professor, E-mail: marco.petrolo@polito.it

^aProfessor, E-mail: erasmo.carrera@polito.it

^bAssistant Professor, E-mail: C.C.deVisser@TUDelft.nl

^cProfessor, E-mail: michele.d_ottavio@u-paris10.fr

^dProfessor, E-mail: Olivier.Polit@u-paris10.fr

platforms, or large boats. Some major technical issues affect helicopters. Such as low forward velocities, the complexity of the main rotor, severe dynamic loadings, noise pollution, and the exposed blades that restrict the accessible areas of helicopters for safety reasons (Johnson 2004).

Many other VTOL aircraft have been proposed over the last decades. In many cases, the propulsion system represents one of the most critical features of the aircraft (Nelms and Anderson 1984). Conventional airplanes are controlled via aerodynamic surfaces, whereas, in a VTOL, the required control forces in sub-aerodynamic flight regimes (e.g., vertical hover) are usually provided by the propulsion system (Curtis 2010). Furthermore, the propulsion system provides lift more often than not. In particular, most VTOLs belong to one of the following categories (Lindenbaum 1986):

- Wingless aircraft in which the propulsion system provides the entire lift.
- Winged aircraft in which the propulsion system provides the required lift as soon as a sufficient cruise speed is reached and lifting surfaces enabled.

A brief overview of some of the main VTOLs developed in the last decades is given hereinafter. Dassault Aviation designed the Mirage III-V and the Balzac V in the mid-1960s (Hirschberg *et al.* 2002). These aircraft had two separated propulsion systems for lift and cruise. Such a strategy was beneficial since each engine set was exploited only for the function it was designed for to optimize its efficiency. The main drawback was due to a large number of engines required for the lift that dramatically reduced the useful payload. A similar strategy was adopted in the Fiat G-222 (1970) (Hirschberg *et al.* 2003). The G-222 was then converted into a Short Take-Off and Landing aircraft (STOL). Such a conversion was beneficial in terms of payload and flyability (Deckert 1995). Another important VTOL category has only one engine set generating both lift and cruise thrust. Such a strategy minimizes the number of thrust-generating devices but requires an adequate system to vector the thrust between the horizontal (cruise flight) and vertical (hover) direction. The Ryan 92 (1959) was a full-metal aircraft in which the trailing edge flaps had to deflect the propeller slipstream. Unfortunately, this aircraft proved to be too heavy to lift without significant head wind. In general, this concept suffers important ground effects that reduce the hovering performances and requires particular pilot skills to control the transition phase and the flight regimes at low power (Nelms and Anderson 1984). Another strategy was the tilt wing configuration, in which the wing carries the tilting engine nacelle. The LTV-Hiller-Ryan XC-142 (1964) was among the first aircraft built according to this strategy but suffered from variable propeller slipstream circulations due to ground effect, longitudinal stability and low directional control power (Knowles 2010). In the tilt shaft configuration, the wing and the nacelle are fixed, only the propeller/rotor shaft is tilted. An example is the Bell XV-3 (1955) that was affected by the dynamic instability of the rotors that caused extremely high cockpit vibrations. The Curtiss-Wright X-19 (1963) was a tilt prop/duct/rotor in which the nacelle carrying the rotor, the propeller or the ducted fan tilted and the wing were kept fixed. This airplane had a very complex and sensitive mechanics. The Bell X-22 (1966) had four tilting ducted fans and served as the basis for the development of a variable stability and control system. Afterward, the Bell XV-15 (1977), the Bell-Boeing V-22 (1989) and the Agusta-Westland AW609 (2003) were developed (Maisel *et al.* 2000). The ERICA project (Enhanced Rotorcraft Innovative Achievement 2000) proposes an outer tilt wing with rotor configuration. In ERICA, the outer wing portion tilts along with the engine nacelle; it is thus a combination of tilt wing and tilt rotor configurations. The key advantages of this concept are the improvement of the hover efficiency and the reduction of the complexity of the tilting mechanism (Bianco-Mengotti 2012). In one case, the Bell 65 Air Test Vehicle (1954), the use of jet thrust was proposed. In a tilt jet, the turbojet engines are fixed under the wing and



Fig. 1 Anuloid geometry

tilted. Another option is the vectored thrust in which the exhausts of a jet engine are oriented through movable nozzles. The transonic ground-attack Hawker-Siddeley AV-8 Harrier (first flight in 1969) was the first VTOL aircraft produced in series.

In many VTOLs, an engine set provides lift and cruise power. Another set provides either supplemental lift (e.g., Yakovlev Yak-38 and F-35B Joint Strike Fighter) or cruise thrust (e.g., Piasecki 16H-1 Pathfinder and Lockheed AH-56 Cheyenne) (Curtis 2010). The vertical and the horizontal thrust can be obtained by ducting the turbojet airflow. One of the first examples of aircraft based on the lift production through a ducted airflow was the VZ-9AV “Avrocar” (1950) (Lindenbaum and Blake). Unfortunately, this aircraft suffered from the ground effect and uncontrolled pitch. The control of the airflow can be realized by movable vanes exploiting the so-called Coanda effect (Barlow *et al.* 2009). The ducted airflow and Coanda effect have recently found increased application in VTOL unmanned aerial vehicles (UAV) (Crivoi *et al.* 2013).

The present paper is a companion work of (Petrolo *et al.* 2014) in which the early development of a disk-shaped VTOL aircraft hereinafter referred to as the Anuloid was presented. In this aircraft, the ducted airflow from a fan powered by a turboshaft contributes to the lift generation together with the Coanda effect that is also exploited for the flight control. This paper presents further developments, with particular attention paid to aerodynamics and flight mechanics.

This paper is organized as follows: the flight mechanics models are described in Section 2, results are given Section 3, and the main conclusions are drawn in Section 4.

2. Flight mechanics models

The Anuloid is a disk-shaped VTOL aircraft, see Fig. 1. The outer diameter is 5 m, and the maximum take-off weight is about 1200 kg. The propulsive system is a turboshaft engine in its center that drives a ducted rotor. Only one propulsion system is implemented for lift and cruise with a more favorable payload-to-empty weight ratio. The typical Anuloid operating scenarios are emergency missions and civil transportations in urban areas. The cruise speed should fall in the 100-200 km/h range. More details about this aircraft can be found in Petrolo *et al.* (2014), (2017).

The equations of motion for rigid aircraft were adapted to be compatible with the unconventional configuration of the aircraft. The equations include the rotational dynamics model, three dynamic damping terms, and a multiplier that allows the scaling of the control moment independently from the aerodynamic moment. The rotational equations of motion are

Table 1 Numerical data on angular momentum of rotor and turbine

Component	Moment of Inertia	Rotation Rate	Angular Momentum
Rotor	$J_{rotor}=0.266 \text{ Kg m}^2$	$\omega_{rotor}=6500 \text{ rpm}$	181.06 Nm s
Turbine	$J_{turbine}=0.274 \text{ Kg m}^2$	$\omega_{turbine}=25500 \text{ rpm}$	731.68 Nm s
Total	-	-	912.73 Nm s

$$\begin{bmatrix} \dot{p} \\ \dot{q} \\ \dot{r} \end{bmatrix} = J^{-1} \begin{bmatrix} K_L \cdot L_{ctrl} + L_{ae} + C_{l_p} \cdot p \\ K_M \cdot M_{ctrl} + M_{ae} + C_{m_q} \cdot q \\ K_N \cdot N_{ctrl} + N_{ae} + C_{n_r} \cdot r \end{bmatrix} + J^{-1} \left(\begin{bmatrix} p \\ q \\ r \end{bmatrix} \times \left(J \begin{bmatrix} p \\ q \\ r \end{bmatrix} + H_{eng} \right) \right) \quad (3)$$

Where p, q, r are the body rotational rates (rad/s), and $\dot{p}, \dot{q}, \dot{r}$ are the body rotational accelerations (rad/s²). The external moments acting on the aircraft are decomposed into aerodynamic components L_{ae}, M_{ae}, N_{ae} (Nm) and control components $L_{ctrl}, M_{ctrl}, N_{ctrl}$ (Nm) which values were obtained from CFD analyses. Furthermore, $K_L \geq 1, K_M \geq 1,$ and $K_N \geq 1$ are the control moment scaling parameters and $C_{l_p} < 0, C_{m_q} < 0,$ and $C_{n_r} < 0$ are the dynamic damping coefficients. Note that the dynamic damping coefficients have a negative value which when multiplied with a positive rate produces a moment in the direction opposite the rotational rates which effectively damps the rotational rate. J is the inertia matrix from CAD,

$$J = \begin{bmatrix} 775.77 & 0.57 & 0 \\ 0.57 & 775.79 & 0 \\ 0 & 0 & 1235.05 \end{bmatrix} \quad (4)$$

The combined angular momentum of the engine is H_{eng} which can be decomposed into two parts

$$H_{eng} = \begin{bmatrix} 0 \\ 0 \\ \omega_{rotor} \cdot J_{rotor} \end{bmatrix} + \begin{bmatrix} 0 \\ 0 \\ \omega_{turbine} \cdot J_{turbine} \end{bmatrix} \quad (5)$$

The values for $\omega_{rotor}, J_{rotor}, \omega_{turbine}, J_{turbine}$ were computed via CAD and given in Table 1. Note that the turbine has a dominant effect on the total angular momentum of the engine system.

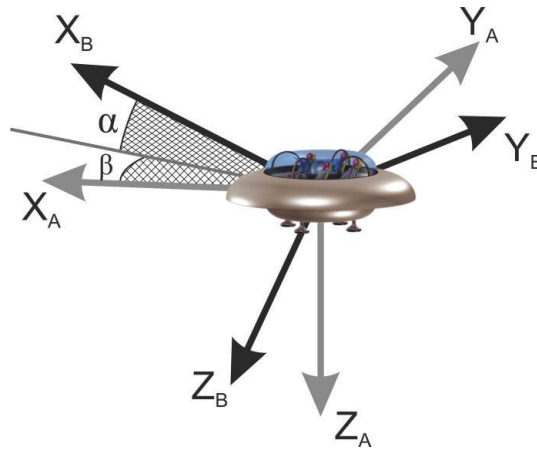
The translational equations of motion are given by

$$\begin{bmatrix} \dot{u} \\ \dot{v} \\ \dot{w} \end{bmatrix} = \frac{1}{m} \begin{bmatrix} X_{ctrl} + X_{ae} \\ Y_{ctrl} + Y_{ae} \\ K_Z \cdot Z_{ctrl} + Z_{ae} \end{bmatrix} + \begin{bmatrix} p \\ q \\ r \end{bmatrix} \times \begin{bmatrix} u \\ v \\ w \end{bmatrix} + g \begin{bmatrix} -\sin \theta \\ \cos \theta \sin \varphi \\ \cos \theta \cos \varphi \end{bmatrix} \quad (4)$$

Where u, v, w are the linear velocities (m/s) in the body axis frame, and $\dot{u}, \dot{v}, \dot{w}$ are the respective linear accelerations (m/s²). The total mass of the aircraft being 1105 kg. The thrust forces $X_{ctrl}, Y_{ctrl}, Z_{ctrl}$ (N) and aerodynamic forces X_{ae}, Y_{ae}, Z_{ae} (N) along the body axes were

Table 2 Proposed aerodynamic model parameters

Parameter	Description	Horizontal flight	Vertical flight
K_L	Roll control moment scaling	4	n/a
K_M	Pitch control moment scaling	4	n/a
K_N	Yaw control moment scaling	1	1
C_{lp}	Dynamic roll Damping (1/s)	-1000	n/a
C_{mq}	Dynamic pitch Damping (1/s)	-1000	n/a
C_{nr}	Dynamic yaw Damping (1/s)	-100	-100
K_Z	Vertical control force scaling	10	1

Fig. 2 Standard aircraft axis definition. Note that the Z_B axis points downwards

calculated using the response surfaces from CFD (Petrolo *et al.* 2014, 2017). The acceleration of gravity is g (9.81 m/s^2). φ , θ are the Euler roll and pitch angles respectively. $K_Z \geq 1$ is the Z-force scaling factor. Note that the X- and Y-forces do not require artificial scaling. In Table 2, the seven proposed parameters are summarized.

The value of the parameters was determined through a tuning procedure that used the control authority as optimization criterion. The total forces and moments acting on the Anuloid are predicted using multivariate polynomial response surfaces which in turn were estimated from CFD results (Petrolo *et al.* 2014, 2017). These response surfaces can be decomposed into their individual polynomial terms. In this case, the decomposition of the total force or moment into an aerodynamic component and a control component is carried out by separating all terms containing the dominant control effector from the total force or moment. For example, for the pitching moment (M) response surface, the dominant control effector is the pitch vane deflection a_{de} , resulting in the following decomposition

$$\begin{aligned}
 M_{tot} &= M_{ctrl} + M_{ae}, \\
 M_{ae} &= c_0 + c_1 V + c_2 F + c_3 \alpha + c_4 V^2 + c_5 F^2 + c_6 \alpha^2 + c_7 VF + c_8 V\alpha + c_9 F\alpha, \\
 M_{ctrl} &= d_0 a_{de} + d_1 a_{de}^2 + d_2 a_{de} V + d_3 a_{de} VF + d_4 a_{de} \alpha
 \end{aligned} \tag{7}$$

For the flight dynamics analysis, a six degrees of freedom dynamic model of the aircraft was created. It is important to note that the aircraft equation of motions are defined in terms of the standard body axis reference frame (Fig. 2), where the X-axis points forward, the Y-axis points to the right, and the Z axis points downwards. For this analysis, a rotor diameter of 1.2 m was used, together with 16 control vanes of length 0.3 m.

The state vector x is defined as follows

$$x = [u \ v \ w \ p \ q \ r \ \varphi \ \theta \ \psi \ \alpha \ \beta \ P_N \ P_E \ h]^T \quad (8)$$

The angle of attack is α , the angle of sideslip is β (both in radians). Finally P_N , P_E , and h , are the North position, the East position, and the altitude respectively (m). The vector of inputs U is defined as follows

$$U = [a_{da} \ a_{de} \ a_{dr} \ V_f]^T \quad (9)$$

Where a_{da} is the deflection angle of the control vanes that produce a rolling moment. a_{de} is the deflection angle of the control vanes that produce a pitching moment. a_{dr} is the deflection angle of the control vanes resulting in a yawing moment (in degrees). The final control variable is V_f which is the volume flow through the rotor (m^3/s).

As shown in (Petrolo *et al.* 2014), the aircraft is statically unstable in the pitch and roll axes. Such instability leads to strongly divergent dynamic behavior in all aircraft states, i.e., the aircraft will very rapidly drift away from (unstable) trim conditions. As a result, open-loop (uncontrolled) analysis during forward flight is only possible within a very short time frame, in this case, less than 1 second. To facilitate a more relevant analysis, linear Proportional-Integral-Differential (PID) and Proportional-Integral (PI) body-rate controllers were included in the aircraft model. Body-rate control uses pilot-defined references for the roll rate (p), pitch rate (q), yaw rate (r) and climb rate (dh/dt) to generate required control surface deflections. These references can be given using standard pilot input devices (stick/yoke+rudder paddles), or by an autopilot outer loop that generates reference body rates to track for example heading and flight path angles.

Starting from the nonlinear moment Eq. (3), a virtual decomposition of the total aerodynamic moments into a control part and an aerodynamic part was carried out,

$$\begin{bmatrix} \dot{p} \\ \dot{q} \\ \dot{r} \end{bmatrix} = J^{-1} \begin{bmatrix} K_L \cdot L_{ctrl}(x, u_L) + L_{ae} + C_{l_p} \cdot p \\ K_M \cdot M_{ctrl}(x, u_M) + M_{ae} + C_{m_q} \cdot q \\ K_N \cdot N_{ctrl}(x, u_N) + N_{ae} + C_{n_r} \cdot r \end{bmatrix} + J^{-1} \left(\begin{bmatrix} p \\ q \\ r \end{bmatrix} \times \left(J \begin{bmatrix} p \\ q \\ r \end{bmatrix} + H_{eng} \right) \right) \quad (10)$$

Where $L_{ctrl}(x, u_L)$, $M_{ctrl}(x, u_M)$, $N_{ctrl}(x, u_N)$ are the control moments calculated using the CFD response surfaces, and u_L , u_M and u_N are the control vane deflection angles.

For the sake of simplicity, a linear relationship between the control moments and the control surfaces was assumed. For example, $M_{ctrl}(x, u_M)$ was assumed a linear function of u_M . Note that while the response surfaces for horizontal flight are known to be quadratic (i.e., nonlinear), the quadratic influence of u_M does not dominate the control moment. As a result, any inaccuracies due to the linearization assumptions will be minimized by the closed loop controller. The linear system assumption does, however, lead to lower performance linear controller compared to a nonlinear controller. Linear control techniques become undesirable or even unfeasible as soon as the nonlinear terms become dominant, or higher control (tracking) performance is required. A solution

Table 3 Controller gains

Roll control		Pitch control		Yaw control		Climb rate control	
Gain	Value	Gain	Value	Gain	Value	Gain	Value
K_{pq}	40	K_{qp}	40	K_{rP}	40	K_{hP}	100
K_{pl}	0	K_{ql}	0	K_{rI}	2.5	K_{hI}	1
K_{pD}	1	K_{qD}	1	K_{rD}	1	K_{hD}	20

would then be to use a gain scheduled, local-linear controller, or otherwise move to nonlinear control strategies such as the nonlinear dynamic inversion (NDI), back-stepping, or incremental methods such as the incremental NDI (INDI), or the sensor based back-stepping (SBB) (Sieberling *et al.* 2010, Sun *et al.* 2014).

For the pitch rate PID controller,

$$u_M(t) = K_{qp}(q_{ref}(t) - q(t)) + K_{qi} \int_0^t (q_{ref}(t) - q(t))dt + K_{qd}(\dot{q}_{ref}(t) - \dot{q}(t)) \quad (11)$$

Where K_{qp} , K_{qi} , and K_{qd} are the proportional gain, the integral gain, and the derivative gain, respectively (see Table 3). The values of these gains must be determined either experimentally or through specific gain tuning methods such as Ziegler-Nichols.

The pitch control moment is then calculated by evaluating the CFD response surface f_{resp} at the pitch rate PID controller $u_M(t)$

$$M_{ctrl}(x, u_M) = f_{resp} \left(x, K_{qp}(q_{ref}(t) - q(t)) + K_{qi} \int_0^t (q_{ref}(t) - q(t))dt + K_{qd}(\dot{q}_{ref}(t) - \dot{q}(t)) \right) \quad (12)$$

Identically, the roll rate controller is given by

$$u_L(t) = K_{rp}(p_{ref}(t) - p(t)) + K_{ri} \int_0^t (p_{ref}(t) - p(t))dt + K_{rd}(\dot{p}_{ref}(t) - \dot{p}(t)) \quad (13)$$

The yaw rate controller is

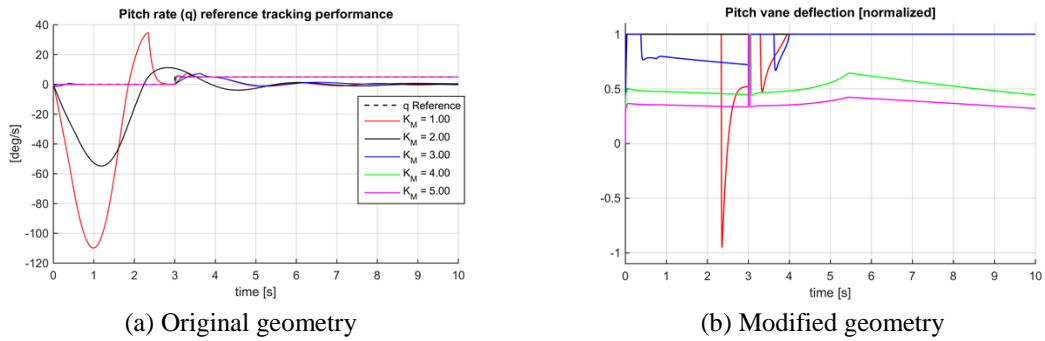
$$u_N(t) = K_{rP}(r_{ref}(t) - r(t)) + K_{rI} \int_0^t (r_{ref}(t) - r(t))dt + K_{rD}(\dot{r}_{ref}(t) - \dot{r}(t)) \quad (14)$$

And finally, the climb rate controller is defined as a PI controller

$$u_h(t) = K_{hP}(\dot{h}_{ref}(t) - \dot{h}(t)) + K_{hI} \int_0^t (\dot{h}_{ref}(t) - \dot{h}(t))dt + K_{hD}(\ddot{h}_{ref}(t) - \ddot{h}(t)) \quad (15)$$

3. Results

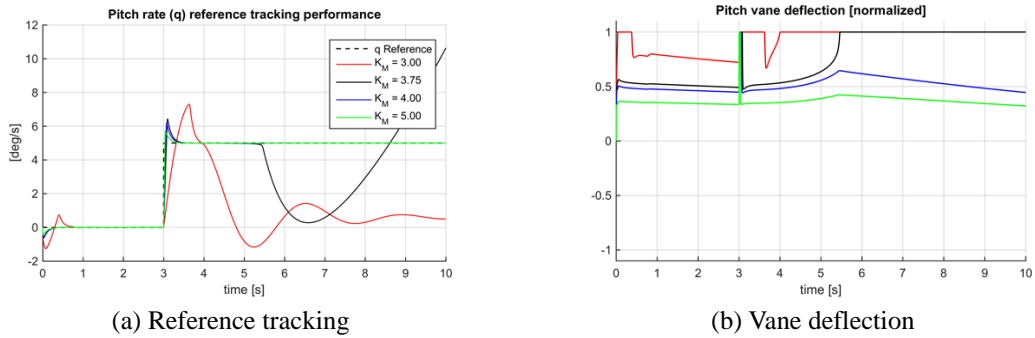
3.1 Horizontal flight control authority analysis



(a) Original geometry

(b) Modified geometry

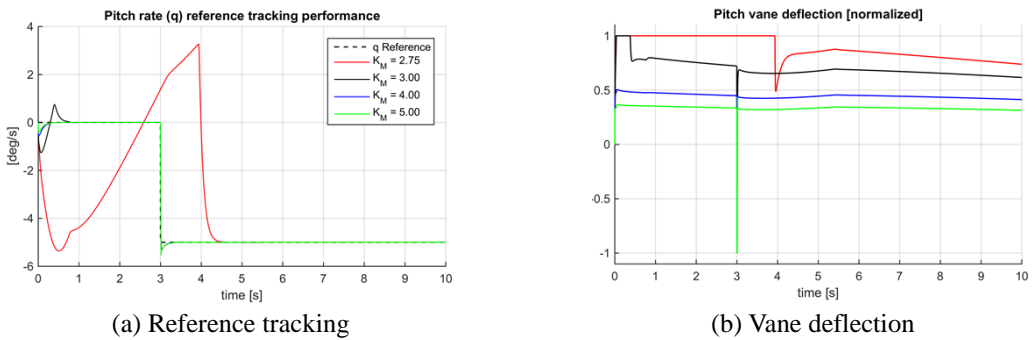
Fig. 3 Pitch rate tracking performance of the aircraft with 5 different values for K_M given a +5 deg/s pitch rate reference at 30 m/s. This figure shows that $K_M > 3$ to prevent pitch control vane saturation. Note that for $K_M < 3$ the aircraft is not capable at all of tracking the reference



(a) Reference tracking

(b) Vane deflection

Fig. 4 Pitch rate tracking performance of the aircraft with 5 different values for K_M given a +5 deg/s pitch rate reference at 30m/s. If $K_M \geq 4$ the pitch control vanes do not saturate after the initial transient for a positive pitch rate reference



(a) Reference tracking

(b) Vane deflection

Fig. 5 Pitch rate tracking performance of the aircraft with 5 different values for K_M given a -5 deg/s (negative) pitch rate reference. If $K_M \geq 3$ the pitch control vanes do not saturate for a negative pitch rate reference beyond the initial transient

The horizontal pitch and roll control authority analysis is presented in this section. In this analysis, a positive or negative pitch and roll rate reference of 5 deg/s and a climb rate of 1 m/s were set as a minimum performance limit. The analysis used a 30 m/s forward velocity for determining the roll, pitch and yaw multiplication factors, and a 10 m/s velocity for determining

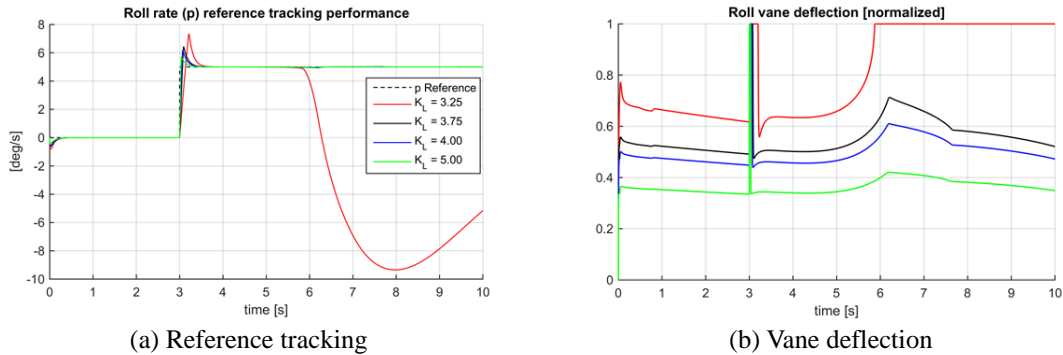


Fig. 6 Roll rate tracking performance of the aircraft with 5 different values for K_L given a 5 deg/s pitch rate reference at 30m/s. If $K_L \geq 3.75$ the pitch control vanes do not saturate for a positive pitch rate reference

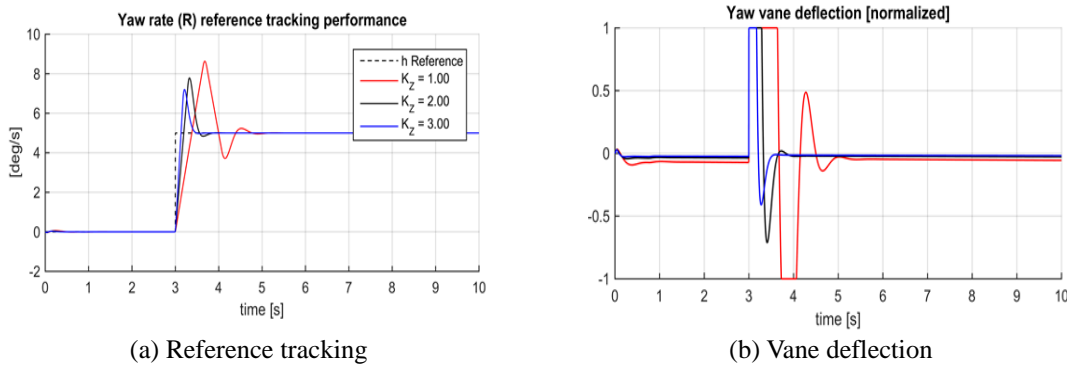


Fig. 7 Yaw rate tracking performance of the aircraft with 3 different values for K_N given a 5 deg/s yaw rate reference at 10 m/s. If $K_N = 1$ the yaw control vanes do not saturate beyond the initial transients

the vertical force multiplication factor. Both velocities produce the most pessimistic results for the respective multiplication factors.

Fig. 3 shows the tracking performance of the 5 deg/s pitch rate reference for values of K_M ranging from 1 to 5. Clearly, if $K_M = 1$ (the nominal aerodynamic model) the reference cannot be followed while the control vanes are completely saturated at their maximum positive deflection, and the aircraft quickly destabilizes and becomes uncontrollable.

Fig. 4 shows a more careful selection of values for K_M . From this figure, it is clear that a positive 5 deg/s pitch rate can be tracked without saturating the control vanes beyond the initial transient when $K_M \geq 3.5$. Interestingly, the effective tracking of negative pitch rates requires a lower K_M than for positive pitch rates, as can be seen in Fig. 5. This can be explained by the tendency of the aircraft to pitch forward, i.e., the pitching moment is asymmetric with respect to the pitch angle. Note that even for higher values of K_M we still see a brief saturation of the pitch vanes during the transient phase of the maneuver. Preventing this saturation is possible, but at the cost of a longer rise time (lower pitch acceleration).

To determine K_L , the rolling moment scaling factor, a similar approach as that taken to determine K_M was considered. The analysis used a roll rate reference of 5 deg/s at a velocity of 30 m/s. In Fig. 6, the results of the analysis are shown. In this case, K_M was fixed to 4 such that unstable pitch dynamics would not influence roll dynamics. In this case, we found that for

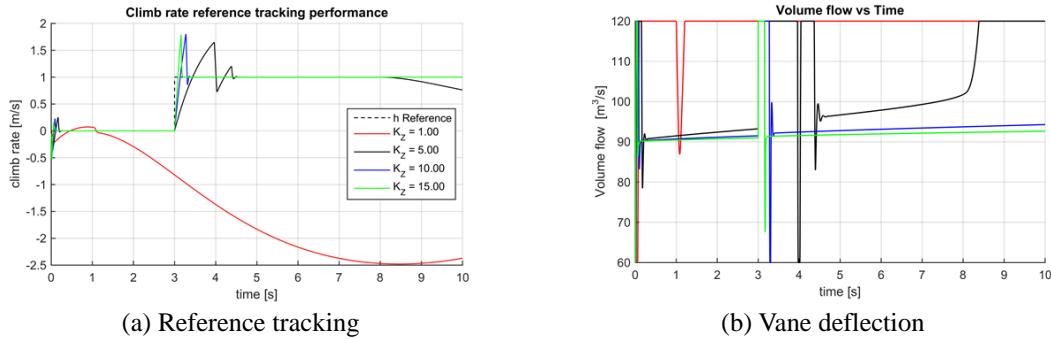


Fig. 8 Climb rate tracking performance of the aircraft with 5 different values for K_Z given a 1 m/s climb rate reference at 30 m/s. If $K_Z \geq 10$ the volume flow does not saturate beyond the transient

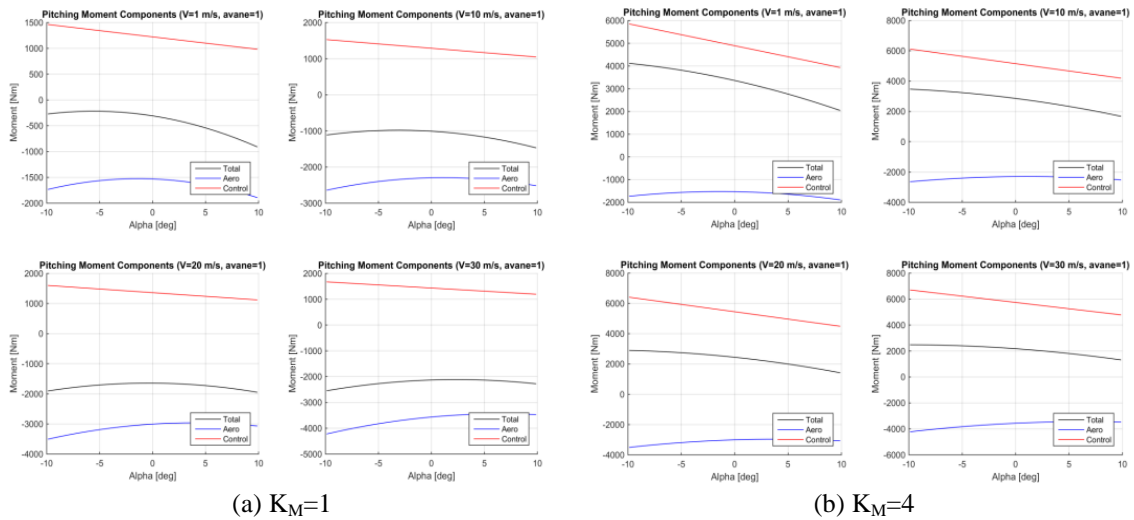


Fig. 9 Pitching moment (factor $K_M=1$) components for maximum positive vane deflection (pitch up)

$K_I \geq 3.25$ accurate roll rate tracking could be achieved without saturating the roll control vanes beyond the initial transient. To determine K_N , the approach above was repeated. From the earlier analysis, it is concluded that the yaw dynamics of the aircraft are both statically and dynamically stable. The yaw rate response for a range of values for K_N between 1 and 3 was analyzed for a yaw rate reference of 5 deg/s and a velocity of 30 m/s. The results of the analysis are shown in Fig. 7, showing that $K_N=1$ leads to desirable yaw dynamics responses. As a result, no scaling factor needs to be imposed on the control yawing moment model.

Finally, the thrust control force scaling K_Z determined using a different approach in the sense that the analysis was performed at 10 m/s as this gave the most pessimistic results. For this analysis, a climb rate controller was used with as reference a 1 m/s positive climb rate. It is found that if $K_Z \geq 10$ a climb rate of 1 m/s can be sustained at a 10 m/s forward velocity, see Fig. 8. The same analysis performed at a velocity of 30 m/s showed that for $K_Z \geq 10$ the 1 m/s climb rate could easily be sustained.

3.2 Static aerodynamic moments during horizontal flight

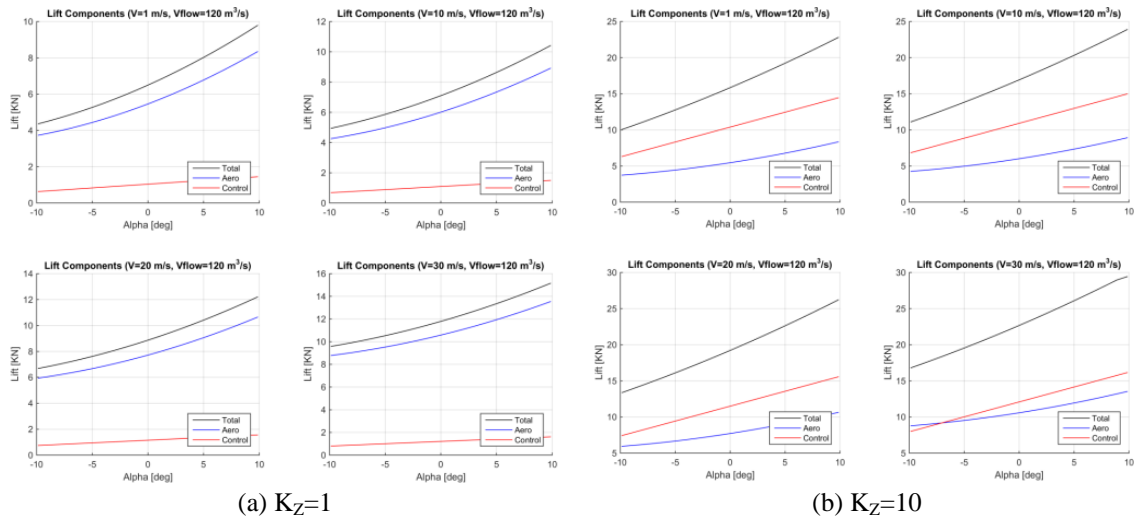


Fig. 10 Lift force components for a volume flow of $120 \text{ m}^3/\text{s}$

An analysis of the scaled aerodynamic forces is provided in this section. The aim of this analysis is to determine whether the scaled aerodynamic moments can still be considered physically valid. In Fig. 9(a), the nominal (unscaled) pitching moment for a maximum positive vane deflection is shown, clearly demonstrating that the total pitching moment is always negative, hence leading to an uncontrollable aircraft. In Fig. 9(b), the pitching moment is again plotted but this time with the scaled moment coefficient factor $K_M=4$. The figure shows that the total pitching moment never exceeds 3000 Nm that is within the range of the nominal moment magnitudes, and can thus be considered physically valid.

3.3 Static aerodynamic forces during horizontal flight

In this section, the lift force before scaling is compared to the lift force after scaling with $K_Z=10$. As discussed in previous sections, this scaling is necessary to allow a climb rate of 1 m/s during forward flight. In Fig. 10(a), the nominal lift force components are plotted. From this figure, it is clear that the magnitude of the volume flow control effector is at least an order of magnitude smaller than the uncontrolled lift component, indicating a very low effectiveness of this control input. In Fig. 10(b), the lift force components are shown after scaling with $K_Z=10$. This time the control component of the lift force is of the same magnitude as the uncontrolled component. The total lift force is significantly higher than that of the unscaled total lift force leading to the conclusion that this scaling may not be physically valid.

3.4 Dynamic forces, moments, and damping

In this section, the results of the dynamic force and moment analysis are presented. These forces and moments are indicative of the forces and moments expected during normal flight. The analysis consisted of two high amplitude pitch rate maneuvers flown at a quasi-stationary 30 m/s trim condition. The analysis uses the modified aircraft aerodynamic database (i.e., $K_L=4$, $K_M=4$, $K_Z=10$). The dynamic damping coefficients were given values such that the order of magnitude of

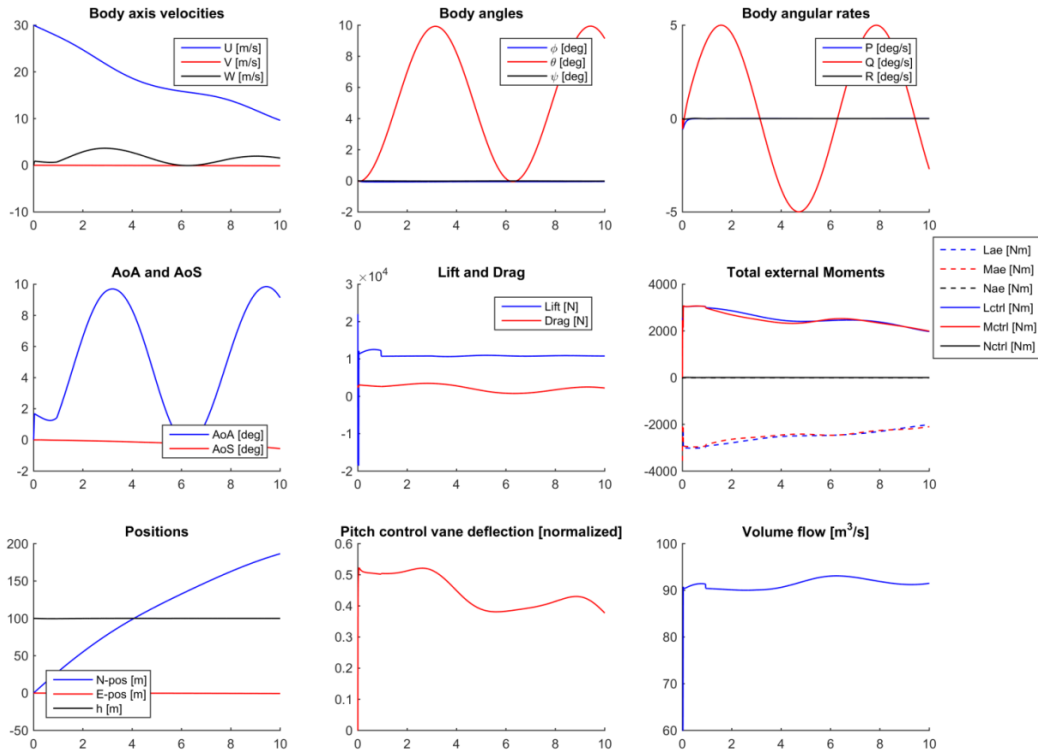


Fig. 11 Aircraft states as function of time for a sine shaped reference on the pitch rate

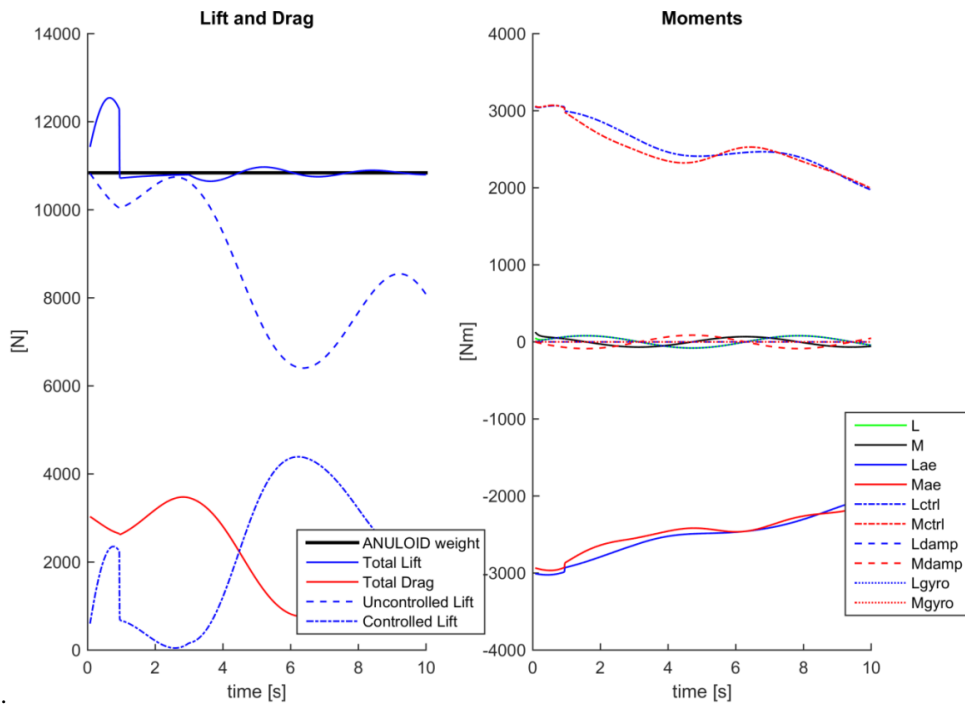


Fig. 12 Decomposition of forces and moments during sine shaped reference on the pitch rate

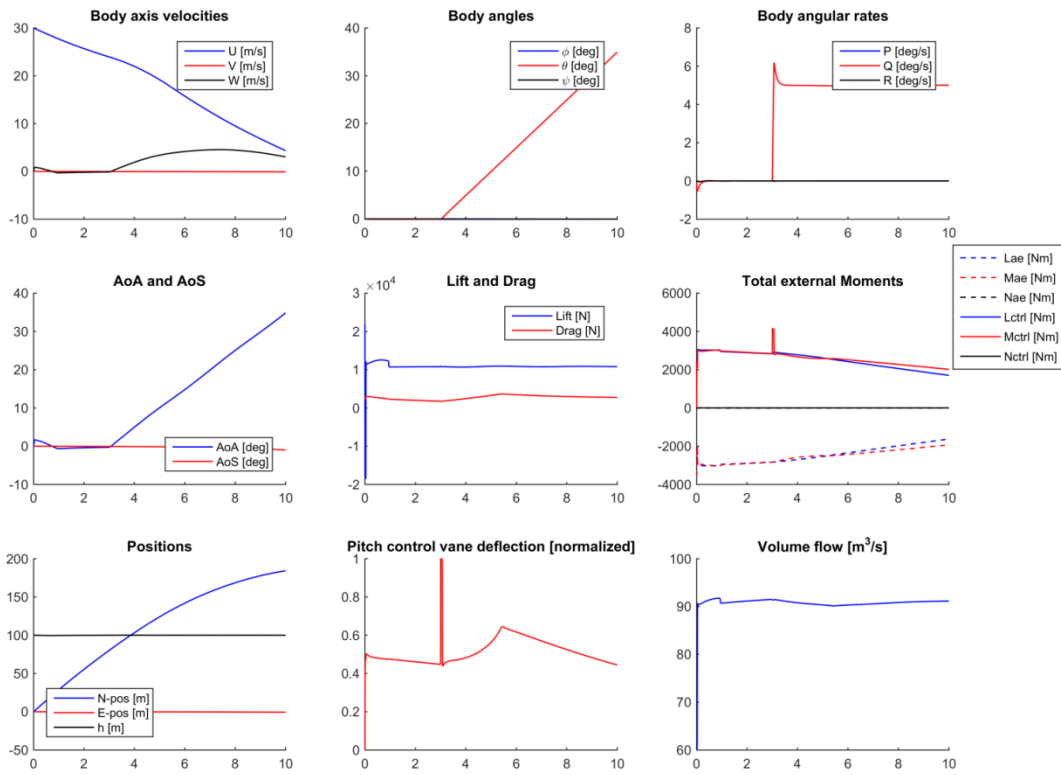


Fig. 13 Aircraft states as function of time for a pitch rate step input

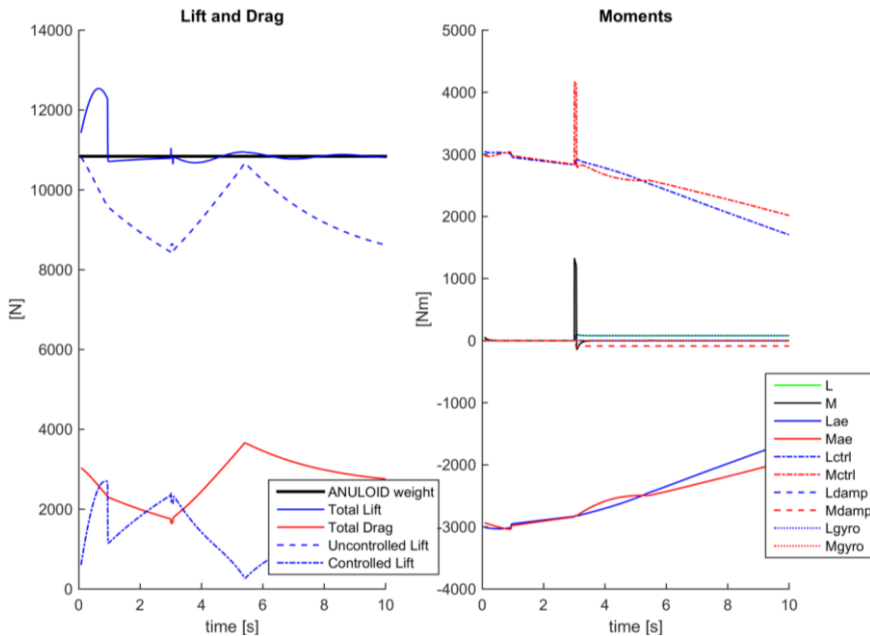


Fig. 14 Dynamic forces and moments acting on the aircraft during a pitch rate tracking task, where a pitch rate of 5 deg/s is tracked after 3 seconds. Notice the sharp peak in the resultant pitching moment during onset of the pitch maneuver

the damping moments was equal to the order of magnitude of the gyroscopic moments. In that case we find $C_{lp}=C_{mq}=-1000$, and $C_{nr}=-100$. Both maneuvers were flown in a closed loop by the automatic control system. The climb rate controller for the engine volume flow was used to keep altitude constant. The first maneuver was a sine shaped reference on the pitch rate. A decomposition of the forces and moments acting on the aircraft during the sine maneuver are shown in Figs. 11 and 12.

The control moments and aerodynamic moments are dominant factors in the decomposition. The dynamic damping peaks at 87 Nm (pitch damping), while gyroscopic moment (rolling moment) peaks at 80 Nm. Note also the relatively low magnitude of the resultant moment which peaks at 128 Nm. The uncontrolled lift forces steadily decrease during this maneuver which is due to the decreasing airspeed. This is compensated for with the climb rate controller that commands a steady increase in thrust. The same analysis was repeated for a step input on the pitch rate, see Figs. 13 and 14.

The control moments and aerodynamic moments again dominate. This time, however, the resultant pitching moment is very significant at 1330 Nm. The dynamic damping peaks at 108 Nm (pitch damping), while gyroscopic moment (rolling moment) peaks at 98 Nm. From the figure, it can be seen that there is a sharp peak in the uncontrolled lift force that is due to the sudden increase in pitch rate. This sharp peak is compensated for by the climb rate controller that aims to keep the climb rate constant.

This analysis shows that while not negligible, dynamic damping and gyroscopic moments are of limited magnitude and do not dominate the flying qualities of Anuloid. Despite this, especially the contribution of the gyroscopic moment cannot be neglected because of its tendency to couple rotations along a given axis to an axis perpendicular to it. For example, a strong pitch up maneuver will lead to a significant moment along the roll axis and vice versa. This coupling must be taken into account during control system design.

6. Conclusions

This paper has presented the main outcomes that stemmed from the development of an innovative disk-shaped VTOL aircraft, the Anuloid. This aircraft is conceived for emergency operations and civil transportation in urban areas. The Anuloid should lower noise pollution (due to the ducted engine) and wider operational scenarios than existing VTOL.

The aircraft is based on the following main characteristics: the lift for take-off and cruise is provided by a fan that is powered by a turboshaft; the anti-torque is provided by a system of fixed and swiveling radial vanes by controlling the swirl of the flow that outgoes from the engine fan; the flight control is obtained by means of the radial vanes and the individually swiveled circumferential vanes.

The results presented in this paper deal with the flight mechanics. The main results are the following:

- The vertical flight characteristics of the aircraft are desirable. The horizontal flight characteristics make the aircraft flyable, but not controllable.
- An in-depth analysis of the pitch and roll authority shows that the control moment components of the total pitch and roll must be amplified by a factor of 4 for the adequate control of the aircraft. Adequacy is defined by its ability to track a 5 deg/s pitch rate and roll rate reference signal.

- The inclusion of dynamic damping terms significantly increases the stability of the aircraft during high amplitude maneuvers. The magnitude of the damping is relatively small compared to the controlled and uncontrolled (aerodynamic) forces and moments.

- The effectiveness of the rotor volume flow as a control effector must be increased by a factor of at least 10.0 to be able to maintain a 1 m/s ascending flight.

Some guidelines and recommendations can be drawn for the future developments of this aircraft. The primary Anuloid issues are the forward flight instability and insufficient control authority. As a general guideline, the reconfiguration of the aircraft should move from a “flying-disk-shaped” to an “aircraft-shaped” Anuloid. This means that, for instance, some primary components should be added, such as lateral wing-like surfaces with movable surfaces and small rotors (both for control and anti-torque capabilities).

Acknowledgments

The research described in this paper was financially supported by the European FP7 project “ANULOID” (ACP2-GA-2013-334861-ANULOID).

References

- Barlow, C., Lewis, D., Prios, S.D., Odedra, S., Erbil, M.A., Karamanoglou, M. and Collis, R. (2009), “Investigating the use of Coanda effect to create novel unmanned aerial vehicles”, *Proceedings of the International Conference on Manufacturing and Engineering Systems*.
- Bianco-Mengotti, R. (2012), *The Agusta Westland Path to the New-Generation Tilt-Rotor*, CESMA-The Future of Rotary Wing, Rome.
- Crivoi, O., Doroftei, I. and Adascalitei, F. (2013), “A survey of unmanned aerial vehicles based on Coanda effect”, *Tehno. J.*, **20**, 338-344.
- Curtis, P. (2010), *VSTOL Integration*, Encyclopedia of Aerospace Engineering.
- Deckert, W. (1995), *The Lift-Fan Aircraft: Lessons Learned*, Nasa Contractor Report, 196694.7
- Federal Aviation Administration (2013), *Noise Certification Standards for Tiltrotors*, 1133-1143.
- Hirschberg, M.J., Müller, T. and Piñero, E. (2003), “Italian V/STOL concepts of the 20th century”, *Proceedings of the American Helicopter Society 59th Annual Forum*.
- Hirschberg, M.J., Müller, T. and Rocher, A. (2002), “French high-speed V/STOL concepts of the 20th century”, *Proceedings of the AIAA International Powered Lift Conference*, Virginia, U.S.A.
- Johnson, W. (2004), *Helicopter Theory*, Dover Publications, New York, U.S.A.
- Knowles, K. (2010), “Introduction to aerial vehicle flight mechanics, stability and control”, *Encyclop. Aerosp. Eng.*
- Lindenbaum, B. (1986), *V/STOL Concepts and Developed Aircraft*, A historical Report (1940-1986), Flight Dynamics Laboratory Report, AFWAL TR 86-3071, **1**.
- Lindenbaum, B. and Blake, W. *The VZ-9 “Avrocar”s*.
- Maisel, M.D., Giulianetti, D.J. and Dugan, C. (2000), *The History Of The Xv-15 Tilt Rotor Research Aircraft: From Concept To Flight*, The NASA History Series, NASA SP-2000-4517.
- Nelms, W.P. and Anderson, S.B. (1984), *V/STOL Concepts in the United States: Past, Present, and Future*, National Aeronautics and Space Administration, Ames Research Center.
- Petrolo, M., Carrera, E., D’Ottavio, M., De Visser, C., Patek, Z. and Janda, Z. (2014), “On the development of the anuloid, a disk-shaped VTOL aircraft for urban areas”, *Adv. Aircraft Spacecraft Sci.*, **1**(3), 353-378.
- Petrolo, M., Carrera, E., Iuso, G., Patek, Z. and Janda, Z. (2017), “Further results on the development of a

- novel VTOL aircraft, the Anuloid, part I: Aerodynamics”, *Adv. Aircraft Spacecraft Sci.*, **4**(4), 401-419.
- Sieberling, S., Chu, Q.P. and Mulder, J.A. (2010), “Robust flight control using incremental nonlinear dynamic inversion and angular acceleration prediction”, *J. Guid. Contr. Dyn.*, **33**(6), 1732-1742.
- Sun, L.G., De Visser, C.C., Chu, Q.P. and Mulder, J.A. (2014), “Joint sensor based backstepping for fault-tolerant flight control”, *J. Guid. Contr. Dyn.*, **38**(1), 62-75.

EC